

The Gemini NICI Planet-Finding Campaign: The Orbit of the Young Exoplanet β Pictoris b

Eric L. Nielsen,¹ Michael C. Liu,¹ Zahed Wahhaj,² Beth A. Biller,³ Thomas L. Hayward,⁴ Jared R. Males,⁵ Laird M. Close,⁵ Katie M. Morzinski,⁵ Andrew J. Skemer,⁵ Marc J. Kuchner,⁶ Timothy J. Rodigas,⁵ Philip M. Hinz,⁵ Mark Chun,¹ Christ Ftaclas,¹ Douglas W. Toomey⁷

ABSTRACT

We present new astrometry for the young (12–21 Myr) exoplanet β Pictoris b taken with the Gemini/NICI and Magellan/MagAO instruments between 2009 and 2012. The high dynamic range of our observations allows us to measure the relative position of β Pic b with respect to its primary star with greater accuracy than previous observations. Based on a Markov Chain Monte Carlo analysis, we find the planet has an orbital semi-major axis of $9.1_{-0.5}^{+5.3}$ AU and orbital eccentricity < 0.15 at 68% confidence (with 95% confidence intervals of 8.2–48 AU and 0.00–0.82 for semi-major axis and eccentricity, respectively, due to a long narrow degenerate tail between the two). We find that the planet has reached its maximum projected elongation, enabling higher precision determination of the orbital parameters than previously possible, and that the planet’s projected separation is currently decreasing. With unsaturated data of the entire β Pic system (primary star, planet, and disk) obtained thanks to NICI’s semi-transparent focal plane mask, we are able to tightly constrain the relative orientation of the circumstellar components. We find the orbital plane of the planet lies between the inner and outer disks: the position angle (PA) of nodes for the planet’s orbit ($211.8 \pm 0.3^\circ$) is 7.4σ greater than the PA of the spine of the outer disk and 3.2σ less than the warped inner disk PA, indicating the disk is not collisionally relaxed. Finally, for the first time we are able to dynamically constrain the mass of the primary star β Pic to $1.76_{-0.17}^{+0.18} M_\odot$.

Subject headings: planets and satellites: detection — stars: individual (β Pic) — planetary systems — planet-disk interactions

¹Institute for Astronomy, University of Hawaii, 2680 Woodlawn Drive, Honolulu, HI 96822, USA

²European Southern Observatory, Alonso de Cordova 3107, Vitacura, Casilla 19001, Santiago, Chile

³Institute for Astronomy, The University of Edinburgh, Royal Observatory, Blackford Hill, Edinburgh EH9 3HJ, UK

⁴Gemini Observatory, Southern Operations Center, c/o AURA, Casilla 603, La Serena, Chile

⁵Steward Observatory, University of Arizona, 933 North Cherry Avenue, Tucson, AZ 85721, USA

⁶Goddard Space Flight Center, Code 667, Greenbelt, MD 20771, USA

⁷Mauna Kea Infrared, LLC, 21 Pookela St., Hilo, HI 96720, USA

1. Introduction

β Pic is a young (~ 12 – 21 Myr, Barrado y Navascués et al. 1999; Zuckerman et al. 2001; Binks & Jeffries 2014), nearby (19.44 pc, van Leeuwen 2007) A6 star that hosts one of the most prominent known debris disks (e.g. Smith & Terrile 1984; Wahhaj et al. 2003; Weinberger et al. 2003; Golimowski et al. 2006; Lagrange et al. 2012a). The disk midplane is warped, with a 4° offset between the inner warped disk and the outer main disk, suggesting a giant planet influencing the disk (Mouillet et al. 1997). This planet β Pic b was first detected in data from 2003, and the planet reappeared on the other side of the star in 2009 (Lagrange et al. 2009, 2010). β Pic b is one of the first planets to be directly imaged and has the smallest projected physical separation of any imaged planet to date. With a contrast of 9 magnitudes at K_S -band and a current projected separation of $\sim 0.4''$, the planet is challenging to detect even with state-of-the-art adaptive optics.

Orbital properties of directly imaged planets can encode clues to their formation. The eccentricities of these planets, for example, may trace migration or planet-planet interactions (e.g., Takeda & Rasio 2005; Jurić & Tremaine 2008; Wang & Ford 2011). β Pic b represents the longest-period exoplanet whose full orbital parameters can be determined with present observations. The estimated orbital period of ~ 20 years allows us the opportunity to determine the orbit of this planet, whereas most other directly imaged planets will require many more decades of observations for a robust orbit determination. The orbital parameters of β Pic b are of particular interest since they allow us to study the relationship between the planet and the debris disk.

The Gemini NICI Planet-Finding Campaign was a 4-year survey to detect extrasolar planets conducted between 2008 and 2012 (Liu et al. 2010; Nielsen et al. 2013; Wahhaj et al. 2013b; Biller et al. 2013). In addition to detecting a number of brown dwarf companions (Biller et al. 2010; Wahhaj et al. 2011; Nielsen et al. 2012), we detected the planet β Pic b at multiple epochs over the course of the Campaign. We combine these observations with new data from Magellan MagAO and previous work to determine the orbit of the planet.

2. Observations

VLT/NACO: Chauvin et al. (2012) present 9 epochs of β Pic b astrometry from VLT NACO, between 2003 and 2011. Bonnefoy et al. (2013) present an additional epoch from January 2012, as well as an improved orbital fit. We use the 10 astrometric observations and errors as reported in these works.

Gemini-South/NICI: We observed β Pic b with NICI at Gemini-South at 4 epochs between 2009 and 2012 (Table 1). Reductions were performed with the Gemini NICI Planet-Finding Campaign pipeline, described in depth in Wahhaj et al. (2013a). These data are discussed in detail in Males et al. (2014), which also includes a comparison to an independent analysis of some of the data by Boccaletti et al. (2013). We find that for overlapping epochs there is good agreement between

the NICI and NACO astrometry, indicating that there is no significant astrometric offset between the two instruments. In addition, NICI measurements have smaller uncertainties compared to those from NACO: the median separation and PA uncertainties are $0.005''$ and 0.6° for NICI and $0.011''$ and 1.81° for NACO. This increased precision is due to the partially transparent focal plane mask of NICI, which allows for an accurate measurement of the location of the star relative to the planet. Bonnefoy et al. (2013) note the primary source of error in their astrometry is the uncertainty in the position of the star.

Magellan/MagAO: β Pic b was observed on UT 2012 December 04 in the Y_S ($0.985 \mu\text{m}$) filter of Magellan MagAO+VisAO, and on UT 2012 December 01, 02, 04, and 07 in the $3.1 \mu\text{m}$, $3.3 \mu\text{m}$, L' , and M' filters of Magellan MagAO+Clio2. The astrometry and photometry from MagAO+VisAO is described in detail in Males et al. (2014) and from MagAO+Clio2 in Morzinski et al. (2014). Similar to NICI, the Magellan MagAO+VisAO instrument has a partially transmissive focal plane mask so the primary star is unsaturated in the data. MagAO+Clio2 data in $3.1 \mu\text{m}$, $3.3 \mu\text{m}$, and L' were taken with long and short exposures of saturated and unsaturated data, while M' data were entirely short unsaturated exposures.

The VisAO astrometry calibration is tied to the wider field of view Clio2 camera, and the two cameras are mounted simultaneously on the same rotator so they will have some common systematics, but the observations of the planet by these two cameras are otherwise independent measurements. To calibrate the Clio2 astrometry, we observed the Trapezium Cluster in the Orion Nebula as a reference. Over the nights of 2012 Dec. 3rd, 4th, 6th, and 8th UT, we locked the AO loop on either θ^1 Ori B or C. Stars θ^1 Ori A and E were also in the fields, as were many fainter Trapezium stars (see Morzinski et al. 2014 for details). We compared the positions of the stars to their positions in Close et al. (2012) to derive the platescale, instrument angle, and distortion solution. We applied these solutions to our β Pic data to calibrate them. The position of the planet was then measured in the Clio2 images by a grid search over (x,y) positions.

3. MCMC Orbit Fitting

3.1. Methods

We use a Metropolis-Hastings Markov Chain Monte Carlo approach to fit orbital parameters to the astrometric motion of β Pic b from 2003 to 2012, following the procedure of Ford (2005) and Ford (2006). Such an approach has previously been applied to astrometric orbits by, e.g., Liu et al. (2008) and Dupuy et al. (2010) for substellar companions, as well as by Chauvin et al. (2012) and Bonnefoy et al. (2013) for β Pic b itself. We compute two types of fits: one with the total system mass fixed (as done by all previous published orbital fits) and another with the total mass as a free parameter. For the fixed-mass case, we have six free parameters: the semi-major axis (a), eccentricity (e), inclination angle (i), argument of periastron (ω), position angle of nodes (Ω), and the epoch of periastron passage (T_0). The period (P) is determined from the semi-major

axis using Kepler’s Third Law and adopting a total system mass of $1.75 M_{\odot}$ (Crifo et al. 1997). For the floating-mass fit, the orbital period is the seventh free parameter, so the total mass is allowed to take on any value.

At the start of the chain, initial values are chosen for each free parameter. A proposed trial step is taken by choosing a displacement in all parameters by randomly drawing from six (or seven) Gaussians centered on the current parameters with fixed standard deviations. The probability ratio between current and proposed orbit parameters is computed by determining the difference in the χ^2 statistic ($\Delta\chi^2$) for all astrometric epochs for β Pic b between the initial and trial sets of parameters. The choice of whether to adopt the trial parameters as the new step or to retain the current set is made via the Metropolis Hastings algorithm with probability ratio $\propto e^{\frac{-\Delta\chi^2}{2}}$. Non-physical parameters ($a \leq 0$, $P \leq 0$, $e < 0$, $e \geq 1$) are assigned a χ^2 of 10^6 while the three viewing angles (i , ω , Ω) and epoch of periastron passage (T_0) are allowed to take any values without limits. To ensure the chains run efficiently, the standard deviations of the Gaussians for choosing trial steps are chosen initially via an iterative procedure where chains are run with different values of standard deviation for each parameter. The standard deviations corresponding to an acceptance rate of 0.25 are used for the final chains (Dupuy et al. 2010).

After we terminate the MCMC chain, the angles are then wrapped around between 0° and 180° for inclination angle, -180° and 180° for argument of periastron, and 0° and 360° for position angle of nodes. Epoch of periastron passage is wrapped around to give a value in the range $[2005, 2005 + \text{period}]$. 2005 is chosen to provide a single distribution of epoch of periastron passage free of discontinuities. Without radial velocity measurements of the star’s reflex motion there is an ambiguity between Ω and $\Omega + 180^\circ$ — that is, whether the south/eastern half of the orbit is closer to the Earth or the north/western half — so while our chains only explored parameter space near $\Omega=212^\circ$, the results are equally valid for $\Omega=32^\circ$.¹

Ten chains are run from the same starting parameters so that we may test for convergence using the Gelman-Rubin (GR) statistic, with 10^8 steps per chain and parameters saved every 1000 steps. The GR statistic is essentially the ratio of the variance in each parameter in individual chains to the total variance for all chains. If each chain is sampling the same region of parameter space then the GR metric will be very close to unity. If the chains are still exploring different regions of parameter space when the chains are terminated, then the GR statistic will be significantly larger than 1. A GR statistic less than 1.1 indicates the chains are converging, while less than 1.01 means excellent convergence (Ford 2006).

¹Lagrange et al. (2012b) present HARPS radial velocity data of β Pic between 2003 and 2010. The RV induced by the activity of the star dominates the expected reflex motion: the measured RV varies between -1.0 and 0.66 km/s with a standard deviation of 0.28 km/s, while the expected RV variation between 2003 and 2011 for the reflex motion of a $10 M_{Jup}$ planet with the median orbital parameters from the MCMC fit is 0.13 km/s. The linear fit to the RV computed by Lagrange et al. (2012b) indicates an increasing RV between 2003 and 2010, consistent with Ω near 212. This orientation is confirmed by the recent measurement of the RV of the planet by Snellen et al. (2014), finding it to be moving toward the Earth at -15.4 ± 1.7 km/s on 17 December 2013 UT.

3.2. Results

We present medians and confidence intervals for each parameter in the fixed-mass case in Table 2. The inclination angle, argument of periastron, position angle of nodes, and epoch of periastron passage have a GR statistic less than 1.01, and the other two parameters have a GR statistic less than 1.1, indicating that our posterior distributions for all parameters are reliable.

Figure 1 displays the resulting marginalized posterior probability distributions for the orbital parameters and total system mass for both the fixed-mass and floating-mass cases. Figure 2 shows an example set of orbital parameters from the fixed-mass MCMC chains that has the lowest χ^2 within the 68% confidence region for all parameters ($\chi^2_{\nu}=1.38$).

Our results for the fixed-mass case show an orbit with semi-major axis of about 9 AU is favored, with inclination angle and position angle of nodes (the two angles that describe the orientation of the orbit on the sky) very tightly constrained and eccentricity mainly <0.2 . Figure 3 shows covariances between some orbital parameters for the fixed-mass fit. There is a strong correlation between eccentricity and semi-major axis, with larger values of semi-major axis corresponding to more eccentric orbits. Given the presence of the disk, it is unlikely that the orbit of the planet is significantly non-circular ($e \gtrsim 0.2$), and we expect future observations to be most consistent with the shorter-period circular orbits from our MCMC chain. With a uniform prior on eccentricity, we find $e < 0.15$ at 68% confidence and $e < 0.72$ at 95% confidence. If we were to impose a prior that eccentricity must be smaller than 0.2, we would obtain $a=8.9_{-0.3}^{+0.8}$ AU and $P=20.1_{-1.2}^{+2.5}$ yr, with the distributions for the other parameters about the same as in the uniform prior case. Our MCMC results find a median of time of maximum elongation (when the projected star-planet separation reaches a maximum) of 2012.63 and 68% (95%) confidence interval between 2012.55 (2012.48) and 2012.70 (2012.79). Our Magellan epochs are after turn around time in 99% of all orbits. So while the Magellan data represent the largest separation between star and planet in our astrometric record, our orbit fitting results indicate that maximum elongation was reached prior to these data being taken.

Finally, we consider the floating-mass MCMC fit. Though generally less constrained than the fixed-mass fit, the posterior mass distribution (lower right panel of Figure 1) shows that the previous estimated mass of $1.75 M_{\odot}$ is well within the 68% confidence interval. While additional astrometry is required to place a more precise limit on the mass of the star β Pic, this total mass distribution of $1.6 \pm 0.3 M_{\odot}$ indicates that our orbital fit and existing astrometric measurements are reasonable. Semi-major axis and period are highly correlated in our floating-mass fit, and while the chains have not converged for semi-major axis and period individually (GR statistics of 1.2), the GR statistic for mass is 1.0012, indicating a reliable measurement of the mass. If we were to impose the prior that $e < 0.2$ in the floating-mass case, our mass constraints for β Pic would slightly tighten to $1.7 \pm 0.2 M_{\odot}$. Similarly, the semi-major axis range would shrink from 24_{-15}^{+51} AU to $9.0_{-0.4}^{+0.9}$ AU. The minimum χ^2 reached in the floating-mass chain (41.64) is similar to that for the fixed-mass chain (41.67).

Crifo et al. (1997) estimate the mass of β Pic by comparing the position of the star on the HR diagram to theoretical evolutionary tracks, finding a good fit for masses between 1.7 and 1.8 M_{\odot} . Blondel & Djie (2006) derive a similar mass, between 1.65 and 1.87 M_{\odot} , again from evolutionary models and the HR diagram. Our dynamical mass is independent of any evolutionary model and so provides independent confirmation of the mass of the star, and indicates these previous estimates were accurate.

3.3. Comparison to Previous Fits

We now compare our results to previously published MCMC orbital fits. Comparing our posteriors to the results from Chauvin et al. (2012), we have similar distributions for semi-major axis and eccentricity but tighter constraints on the viewing angles of the orbit. For inclination angle and position angle of nodes, we find $88.9 \pm 0.7^{\circ}$ and $211.8 \pm 0.3^{\circ}$ compared to $88.5 \pm 1.7^{\circ}$ and $212.6 \pm 1.5^{\circ}$ from Chauvin et al. We find similar distributions in semi-major axis and eccentricity, though with smoother posteriors indicating our MCMC chains are better converged. (Chauvin et al. do not provide GR values for their fit but state that their GR statistics are consistent with convergence.) Since the preferred orbits from our chains are close to circular (68% having eccentricity less than 0.15), the argument of periastron and epoch of periastron passage are poorly defined as they were for Chauvin et al., since it is difficult to determine periastron in a near-circular orbit. Nevertheless, the two values are tightly correlated (bottom right panel of Figure 3). While the location of periastron is not well-defined, the location of the planet at a particular epoch between ~ 2000 and ~ 2020 is.

Bonnefoy et al. (2013) refit the orbit with data from Chauvin et al. (2012) as well as an additional VLT data point from 2012 and find similar results, with MCMC chains that appear more converged than those of Chauvin et al. (2012). The semi-major axis from this fit is reported to be within 8–10 AU at 80% confidence; we find a less constrained semi-major axis, with 80% confidence lying between 8 and 14 AU. We also find a wider range of eccentricities that fit the data, with 80% confidence $e < 0.35$ compared to $e < 0.15$ reported by Bonnefoy et al. (2013). Conversely, we find tighter constraints on the orientation of the orbit on the sky. From their Figure 8, we determine that their inclination angle distribution is centered on 88.7° with a FWHM of 3.5° , and their distribution for position angle of nodes is centered on 212° and FWHM of 2.7° . Our distributions for these parameters have similar centers of 88.9° and 211.8° , but with smaller FWHMs of 1.7° and 0.7° .

After our paper was submitted, Macintosh et al. (2014) presented an additional measurement of the position of β Pic b on 18 November 2013 UT, measuring $0.434 \pm 0.006''$ and $211.8 \pm 0.5^{\circ}$, using the Gemini Planet Imager (GPI) at Gemini-South. They fit this new datapoint along with the VLT astrometry presented in Chauvin et al. (2012). Their astrometric coverage thus has a 3-year gap between early 2011 and late 2013, and a datapoint one year later than the orbital coverage we present here. They find generally similar results for orientation of the orbit, $\Omega = 211.6 \pm 0.45^{\circ}$

and $i = 90.69 \pm 0.68^\circ$ compared to $211.8 \pm 0.3^\circ$ and $88.9 \pm 0.7^\circ$ we present here. The peaks of their distributions for semi-major axis and eccentricity are similar to ours, but their posteriors do not reveal the same narrow degenerate tail toward large eccentricity and large semi-major axis. (Note that Macintosh et al. 2014 plot 10, 50, and 90% confidence contours for their orbit fitting results, while we show 68.3, 95.4, and 99.7% contours.)

When we fit their data (the combination of the Chauvin et al. 2012 and the GPI astrometry) with our MCMC method, we do not reproduce the posteriors of Macintosh et al. (2014) and still see the same long eccentricity tail. In fact, the lowest chi-square orbit reached in the chain is in this tail ($\chi^2_\nu = 0.45$), with semi-major axis 47.8 AU and eccentricity of 0.81. The cause of this discrepancy is most likely the choice of priors, as a non-uniform prior on eccentricity can make high eccentricity orbits sufficiently unlikely so that the chain never leaves the low-period, low-eccentricity region of parameter space. For other orbital parameters, including inclination angle (with a reflection about 90°) and position angle of nodes, we precisely reproduce the 68% confidence intervals given by Macintosh et al. (2014).

Finally, we combine our dataset with the additional GPI astrometry point and re-fit the orbit. We find similar parameters for the fixed-mass case as we present here, $a = 9.4^{+11.8}_{-0.6}$ and $e = 0.09^{+0.49}_{-0.06}$, with the same degenerate tail toward long periods and large eccentricities as before. We find slightly smaller error bars for inclination angle and position angle of nodes, $i = 89.1 \pm 0.6^\circ$ and $\Omega = 211.4 \pm 0.24^\circ$. While the 68% confidence intervals are largely unchanged for these parameters, in the floating-mass case we significantly reduce the uncertainty on the mass of β Pic, $M = 1.76^{+0.18}_{-0.17} M_\odot$, reaching 10% precision on the mass of the star.²

4. Disk-Planet Alignment

In order to compare the position angle of the orbit to the disk, we perform a custom reduction of our 2011 NICI data to recover the disk. We begin by removing the azimuthally averaged profile of the point spread function from the individual images, as described in Wahhaj et al. (2013a) except that the running azimuthal average used here is taken over 90 pixels instead of 30 pixels. This process removes large scale (>90 pixels or $1.62''$) azimuthal structure from both the stellar halo and the disk. Since the β Pic disk is known to be edge-on, this procedure does not alter the disk profile significantly. After this step the disk reduction then proceeds with our standard ADI

²Using our MCMC fit to the dataset presented here (VLT, NICI, and Magellan data) we would predict astrometry on 18 November 2013 of $0.415 \pm 0.007''$ and $212.3 \pm 0.6^\circ$, within 1.5 and 0.1 σ of the GPI measurements, respectively. For the floating mass case the predicted positions are $0.424 \pm 0.019''$ and $212.3 \pm 0.6^\circ$. The uncertainty in our predictions and the GPI measurement errors are similar for the fixed mass case, though with a slight offset in separation, so it is not surprising that adding the GPI datapoint to this analysis does not produce substantially different results. For the floating mass case, however, the prediction uncertainty for separation is three times larger than the measurement error, so the new point does noticeably refine the fit.

pipeline.

The signal-to-noise maps of the reduced images for the CH_4L and K_{cont} filters are shown in Figure 4. The North/East (NE) and the South/West (SW) extensions of the disk were considered separately. As a function of radius we fit two Gaussians to the azimuthal disk profile, taking a 20 AU width at each sampling and stepping by 1 AU. We compute the median position angles for the two sides of the outer disk (between 60 and 120 AU) of $209.21 \pm 0.05^\circ$ and $28.79 \pm 0.06^\circ$. The inner disk is only visible within 90 AU, and we find median values of the position angle between 60 and 90 AU of $212.99 \pm 0.07^\circ$ and $32.28 \pm 0.07^\circ$. These are errors in the fit only and do not include uncertainty in the position of north of 0.2° , as we are concerned only with the relative offset between the orbital plane of the planet and the position angle of the disk. We present these values along with relative and absolute errors in Table 3.

To ensure that our reduction process has not biased these measurements we simulate the disk as a series of rings given the fit to the data, and then create a simulated dataset with the same set of rotation angles in our ADI dataset (a total range of 42 degrees) to model self-subtraction. The offset between the initial model and the measurements of the self-subtracted simulation was much smaller than 0.1° , and so this effect is not the dominant source of error. Rather it is residuals from the stellar point spread function that dominate the measurement of the disk position angle.

Our PA measurements are consistent with the cADI 2-component fit reported by Lagrange et al. (2012a), who find $29.07^\circ_{-0.19}^{+0.20}$ and $209.00^\circ_{-0.15}^{+0.16}$ for the outer disk. Our measurements of offsets between outer and inner disk of $3.78 \pm 0.12^\circ$ (SW) and $3.49 \pm 0.13^\circ$ (NE) are also close to the Lagrange et al. (2012a) cADI value of $3.9_{-0.1}^{+0.6^\circ}$. Unlike Lagrange et al. (2012a), where the position of the center of the star is uncertain, the partially transmissive focal plane mask of NICI allows us to precisely measure the star position in images of the disk.

Using our position angle for the SW disk of $209.21 \pm 0.05^\circ$, our measurement of the position angle of nodes of the orbit of $211.8 \pm 0.3^\circ$ is 7.4σ discrepant with the position angle of the outer disk. The inner warped disk has a position angle of $212.9 \pm 0.07^\circ$, which is discrepant at the 3.2σ level. Thus, we find the planet’s orbital plane is not aligned with either disk.

Currie et al. (2011) presented a preliminary orbit based on four astrometric points (the bare minimum needed for an orbit fit) and a non-MCMC method and found the position angle of nodes to be between the two disks. When we apply our MCMC method to their data we find generally larger uncertainties in orbital parameters than Currie et al. (2011) report. Using an MCMC fit to their data, we find the position angle of nodes to be $210.9 \pm 0.9^\circ$, 1.8σ greater than the outer disk PA and 2.2σ less than the inner disk PA. Chauvin et al. (2012) and Bonnefoy et al. (2013) fit more data with a similar MCMC method to ours and find the orbital plane of the planet to be consistent with the inner disk ($\Omega=212.6 \pm 1.5^\circ$ and $\Omega=212.0 \pm 1.1^\circ$, respectively, both within 1σ of the PA of the inner disk). By including our higher precision astrometric data and longer time baseline, we find the position angle of nodes to be between the two disks, though closer to the inner disk.

5. Discussion

We now consider the implications of a misalignment between β Pic b and the two disks. Our observations recall a dynamical picture of the β Pic disk recently painted by Dawson et al. (2011). If a planet on an inclined orbit (inclination i_p) is introduced into a disk of non-interacting particles with zero initial inclination, the secular theory of Laplace-Lagrange (e.g. Murray & Dermott 1999) show us that the inclinations of the particles will oscillate about i_p , creating a cuspy disk structure with apparent inclination $2i_p$ in its inner regions. Our measurement that the planet’s inclination is intermediate between the two observed disk planes seems to support this picture. In contrast, earlier simulations by Mouillet et al. (1997) and Augereau et al. (2001) yielded a disk coplanar with the planet.

One important assumption built into the Dawson et al. (2011) model and supported by our observations is that the planetesimals are not yet collisionally relaxed (collisional relaxation in debris disks is the gradual process by which planetesimals lose energy and exchange momentum via collisions so that the distribution of their orbits approaches a steady state), as models of structure in other debris disks have assumed (e.g. Quillen 2006, Rodigas et al. 2014). Another important assumption built into the Dawson et al. (2011) model is that the planet is introduced instantaneously, fully formed, at time zero. We infer that the β Pic disk is probably not collisionally relaxed; this inference should yield some interesting constraints on models of the collisional evolution of planetesimals in debris disks (e.g. Nesvold et al. 2013). Moreover, if the Dawson et al. (2011) model is indeed correct, it appears that the β Pic planet was introduced to its current orbit suddenly compared to the secular time scale, perhaps scattered there by another planet.

This notion begs us to ponder the role of multiple planets in sculpting the disk. In the context of their model, Dawson et al. (2011) placed severe limits on the presence of a second planet in the system disturbing the disk. In addition, Absil et al. (2013) exclude a second planet more massive than $\sim 5 M_{Jup}$ outside of $0.2''$ based on L' high contrast images of β Pic. But what caused the inclination of β Pic b if not an interaction with another massive planet? And how did the planetesimals respond to this interaction? These questions remain unanswered.

Finally, we consider the transit event noted by Lecavelier Des Etangs et al. (1995) in November 1981 and find very loose constraints on a transit of the planet given the available data. We search for such a transit by finding the smallest projected distance between star and planet between 2015 and 2019 and then subtract one or two orbital period from the returned epoch for each step in our MCMC chains, choosing the epochs that are closest to 1981. We find the most recent closest approach to be at epoch $2007.44_{-0.17}^{+0.14}$ (crossing behind the star), with the next closest approach to take place in $2017.59_{-0.18}^{+0.60}$, adopting the orientation of the orbit from the RV measurements of Lagrange et al. (2012b) and Snellen et al. (2014) (see footnote 1). The median value for the epoch of closest approach one or two orbital period earlier than 2017 is 1977.52, with a 68% confidence interval between 1971.07 and 1982.14 (95% confidence between 1768 and 1993, given the long tail of the posterior for orbital period). The smallest projected distance from star to planet is less than

31 times the radius of β Pic ($1.8 \pm 0.2 R_{\odot}$); Di Folco et al. 2004) at 68% confidence (<51 times the radius at 95% confidence). Thus we cannot rule out a transit with the current orbital fit. Lecavelier Des Etangs et al. (1995) and Chauvin et al. (2012) speculate that the transit event may not be caused by the planet itself but rather by solid material entrained by the planet and carried in its Hill sphere. We cannot rule out this possibility either, and more data are required. We predict that the next transit will take place between 2017.41 and 2018.18 at 68% confidence (2017.27–2019.19 at 95% confidence), with a median epoch of 2017.59. Additional astrometric observations in the next few years will provide a more precise transit window and transit probability.

6. Conclusions

We have examined the orbit of β Pic b given five new epochs of data taken with Gemini/NICI and Magellan/MagAO, finding a semi-major axis of $9.1_{-0.5}^{+5}$ AU and a period of 21_{-2}^{+21} years. The astrometric record of β Pic b is now long enough to be able to remove the assumption of the total system mass, which was needed by all previous fits to this orbit. When we solve for the mass of β Pic itself we find a value of $1.76_{-0.17}^{+0.18} M_{\odot}$, consistent with the expected value of $1.75 M_{\odot}$. The position angle of nodes for our fixed-mass orbit is offset from the observed position angles of the inner warped disk (at 3.2σ significance) and from the outer disk (at 7.4σ significance), suggesting that the disk is not collisionally relaxed.

Numerous degenerate orbital solutions exist for astrometric data that show minimal acceleration during the timeframe of the observations, in particular between semi-major axis, period, and eccentricity. Observing significant acceleration, and in particular the reversal of direction at maximum elongation, greatly reduces these degeneracies. Our orbital fit indicates that the planet has reached maximum elongation and is currently moving back toward the star, crossing to the other side of the star by ≈ 2018 . β Pic b has been observed extensively since its reappearance in 2009 and the current window for studying the planet will remain open for just a few more years before the planet is undetectable behind the star again. Advanced planet-finding instruments such as GPI and SPHERE will likely allow for orbital monitoring of the planet closer to the star, so the time of lost contact is likely to be significantly shorter than it was between 2003 and 2009. The window for the next transit is between 2017.41 and 2018.18 at 68% confidence, and future astrometric monitoring will provide a more precise prediction to guide photometric monitoring.

We thank Jessica Lu and Adam Kraus for helpful discussions. B.A.B was in part supported by Hubble Fellowship grant HST-HF-01204.01-A awarded by the Space Telescope Science Institute, which is operated by AURA for NASA under contract NAS 5-26555. This work was supported in part by NSF grants AST-0713881 and AST-0709484 awarded to M. Liu. The Gemini Observatory is operated by the Association of Universities for Research in Astronomy, Inc., under a cooperative agreement with the NSF on behalf of the Gemini partnership: the National Science Foundation (United States), the Science and Technology Facilities Council (United Kingdom), the National Research Council (Canada), CONICYT (Chile), the Australian Research Council (Aus-

tralia), CNPq (Brazil), and CONICET (Argentina). This research has made use of the SIMBAD database, operated at CDS, Strasbourg, France.

Facilities: Gemini:South (NICI), Magellan II (MagAO+Clio2), Magellan II (MagAO+VisAO).

REFERENCES

- Absil, O., Milli, J., Mawet, D., Lagrange, A.-M., Girard, J., Chauvin, G., Boccaletti, A., Delacroix, C., & Surdej, J. 2013, *A&A*, 559, L12
- Augereau, J. C., Nelson, R. P., Lagrange, A. M., Papaloizou, J. C. B., & Mouillet, D. 2001, *A&A*, 370, 447
- Barrado y Navascués, D., Stauffer, J. R., Song, I., & Caillault, J.-P. 1999, *ApJ*, 520, L123
- Biller, B. A., Liu, M. C., Wahhaj, Z., Nielsen, E. L., Close, L. M., Dupuy, T. J., Hayward, T. L., Burrows, A., Chun, M., Ftaclas, C., Clarke, F., Hartung, M., Males, J., Reid, I. N., Shkolnik, E. L., Skemer, A., Tecza, M., Thatte, N., Alencar, S. H. P., Artymowicz, P., Boss, A., de Gouveia Dal Pino, E., Gregorio-Hetem, J., Ida, S., Kuchner, M. J., Lin, D., & Toomey, D. 2010, *ApJ*, 720, L82
- Biller, B. A., Liu, M. C., Wahhaj, Z., Nielsen, E. L., Hayward, T. L., Males, J. R., Skemer, A., Close, L. M., Chun, M., Ftaclas, C., Clarke, F., Thatte, N., Shkolnik, E. L., Reid, I. N., Hartung, M., Boss, A., Lin, D., Alencar, S. H. P., de Gouveia Dal Pino, E., Gregorio-Hetem, J., & Toomey, D. 2013, *ApJ*, 777, 160
- Binks, A. S. & Jeffries, R. D. 2014, *MNRAS*, 438, L11
- Blondel, P. F. C. & Djie, H. R. E. T. A. 2006, *A&A*, 456, 1045
- Boccaletti, A., Lagrange, A.-M., Bonnefoy, M., Galicher, R., & Chauvin, G. 2013, *A&A*, 551, L14
- Bonnefoy, M., Boccaletti, A., Lagrange, A.-M., Allard, F., Mordasini, C., Beust, H., Chauvin, G., Girard, J. H. V., Homeier, D., Apai, D., Lacour, S., & Rouan, D. 2013, *A&A*, 555, A107
- Chauvin, G., Lagrange, A.-M., Beust, H., Bonnefoy, M., Boccaletti, A., Apai, D., Allard, F., Ehrenreich, D., Girard, J. H. V., Mouillet, D., & Rouan, D. 2012, *A&A*, 542, A41
- Close, L. M., Puglisi, A., Males, J. R., Arcidiacono, C., Skemer, A., Guerra, J. C., Busoni, L., Brusa, G., Pinna, E., Miller, D. L., Riccardi, A., McCarthy, D. W., Xompero, M., Kulesa, C., Quiros-Pacheco, F., Argomedo, J., Brynnel, J., Esposito, S., Mannucci, F., Boutsia, K., Fini, L., Thompson, D. J., Hill, J. M., Woodward, C. E., Briguglio, R., Rodigas, T. J., Briguglio, R., Stefanini, P., Agapito, G., Hinz, P., Follette, K., & Green, R. 2012, *ApJ*, 749, 180

- Crifo, F., Vidal-Madjar, A., Lallement, R., Ferlet, R., & Gerbaldi, M. 1997, *A&A*, 320, L29
- Currie, T., Thalmann, C., Matsumura, S., Madhusudhan, N., Burrows, A., & Kuchner, M. 2011, *ApJ*, 736, L33
- Dawson, R. I., Murray-Clay, R. A., & Fabrycky, D. C. 2011, *ApJ*, 743, L17
- Di Folco, E., Thévenin, F., Kervella, P., Domiciano de Souza, A., Coudé du Foresto, V., Ségransan, D., & Morel, P. 2004, *A&A*, 426, 601
- Dupuy, T. J., Liu, M. C., Bowler, B. P., Cushing, M. C., Helling, C., Witte, S., & Hauschildt, P. 2010, *ApJ*, 721, 1725
- Ford, E. B. 2005, *AJ*, 129, 1706
- . 2006, *ApJ*, 642, 505
- Golimowski, D. A., Ardila, D. R., Krist, J. E., Clampin, M., Ford, H. C., Illingworth, G. D., Bartko, F., Benítez, N., Blakeslee, J. P., Bouwens, R. J., Bradley, L. D., Broadhurst, T. J., Brown, R. A., Burrows, C. J., Cheng, E. S., Cross, N. J. G., Demarco, R., Feldman, P. D., Franx, M., Goto, T., Gronwall, C., Hartig, G. F., Holden, B. P., Homeier, N. L., Infante, L., Jee, M. J., Kimble, R. A., Lesser, M. P., Martel, A. R., Mei, S., Menanteau, F., Meurer, G. R., Miley, G. K., Motta, V., Postman, M., Rosati, P., Sirianni, M., Sparks, W. B., Tran, H. D., Tsvetanov, Z. I., White, R. L., Zheng, W., & Zirm, A. W. 2006, *AJ*, 131, 3109
- Jurić, M. & Tremaine, S. 2008, *ApJ*, 686, 603
- Lagrange, A.-M., Boccaletti, A., Milli, J., Chauvin, G., Bonnefoy, M., Mouillet, D., Augereau, J. C., Girard, J. H., Lacour, S., & Apai, D. 2012a, *A&A*, 542, A40
- Lagrange, A.-M., Bonnefoy, M., Chauvin, G., Apai, D., Ehrenreich, D., Boccaletti, A., Gratadour, D., Rouan, D., Mouillet, D., Lacour, S., & Kasper, M. 2010, *Science*, 329, 57
- Lagrange, A.-M., De Bondt, K., Meunier, N., Sterzik, M., Beust, H., & Galland, F. 2012b, *A&A*, 542, A18
- Lagrange, A.-M., Gratadour, D., Chauvin, G., Fusco, T., Ehrenreich, D., Mouillet, D., Rousset, G., Rouan, D., Allard, F., Gendron, É., Charton, J., Mugnier, L., Rabou, P., Montri, J., & Lacombe, F. 2009, *A&A*, 493, L21
- Lecavelier Des Etangs, A., Deleuil, M., Vidal-Madjar, A., Ferlet, R., Nitschelm, C., Nicolet, B., & Lagrange-Henri, A. M. 1995, *A&A*, 299, 557
- Liu, M. C., Dupuy, T. J., & Ireland, M. J. 2008, *ApJ*, 689, 436

- Liu, M. C., Wahhaj, Z., Biller, B. A., Nielsen, E. L., Chun, M., Close, L. M., Ftaclas, C., Hartung, M., Hayward, T. L., Clarke, F., Reid, I. N., Shkolnik, E. L., Tecza, M., Thatte, N., Alencar, S., Artymowicz, P., Boss, A., Burrows, A., de Gouveia Dal Pino, E., Gregorio-Hetem, J., Ida, S., Kuchner, M. J., Lin, D., & Toomey, D. 2010, in Society of Photo-Optical Instrumentation Engineers (SPIE) Conference Series, Vol. 7736, Society of Photo-Optical Instrumentation Engineers (SPIE) Conference Series
- Macintosh, B., Graham, J. R., Ingraham, P., Konopacky, Q., Marois, C., Perrin, M., Poyneer, L., Bauman, B., Barman, T., Burrows, A., Cardwell, A., Chilcote, J., De Rosa, R. J., Dillon, D., Doyon, R., Dunn, J., Erikson, D., Fitzgerald, M., Gavel, D., Goodsell, S., Hartung, M., Hibon, P., Kalas, P. G., Larkin, J., Maire, J., Marchis, F., Marley, M., McBride, J., Millar-Blanchaer, M., Morzinski, K., Norton, A., Oppenheimer, B. R., Palmer, D., Patience, J., Pueyo, L., Rantakyro, F., Sadakuni, N., Saddlemyer, L., Savransky, D., Serio, A., Soummer, R., Sivaramakrishnan, A., Song, I., Thomas, S., Wallace, J. K., Wiktorowicz, S., & Wolff, S. 2014, ArXiv e-prints
- Males, J. R., Close, L. C., Morzinski, K. M., Wahhaj, Z., Liu, M. C., et al. 2014, accepted ApJ
- Morzinski, K. M., Close, L. C., Males, J. R., et al. 2014, in prep. ApJ
- Mouillet, D., Larwood, J. D., Papaloizou, J. C. B., & Lagrange, A. M. 1997, MNRAS, 292, 896
- Murray, C. D. & Dermott, S. F. 1999, Solar system dynamics
- Nesvold, E. R., Kuchner, M. J., Rein, H., & Pan, M. 2013, ApJ, 777, 144
- Nielsen, E. L., Liu, M. C., Wahhaj, Z., Biller, B. A., Hayward, T. L., Boss, A., Bowler, B., Kraus, A., Shkolnik, E. L., Tecza, M., Chun, M., Clarke, F., Close, L. M., Ftaclas, C., Hartung, M., Males, J. R., Reid, I. N., Skemer, A. J., Alencar, S. H. P., Burrows, A., de Gouveia Dal Pino, E., Gregorio-Hetem, J., Kuchner, M., Thatte, N., & Toomey, D. W. 2012, ApJ, 750, 53
- Nielsen, E. L., Liu, M. C., Wahhaj, Z., Biller, B. A., Hayward, T. L., Close, L. M., Males, J. R., Skemer, A. J., Chun, M., Ftaclas, C., Alencar, S. H. P., Artymowicz, P., Boss, A., Clarke, F., de Gouveia Dal Pino, E., Gregorio-Hetem, J., Hartung, M., Ida, S., Kuchner, M., Lin, D. N. C., Reid, I. N., Shkolnik, E. L., Tecza, M., Thatte, N., & Toomey, D. W. 2013, ApJ, 776, 4
- Quillen, A. C. 2006, MNRAS, 372, L14
- Rodigas, T. J., Malhotra, R., & Hinz, P. M. 2014, ApJ, 780, 65
- Smith, B. A. & Terrile, R. J. 1984, Science, 226, 1421
- Snellen, I., Brandl, B., de Kok, R., Brogi, M., Birkby, J., & Schwarz, H. 2014, ArXiv e-prints

- Takeda, G. & Rasio, F. A. 2005, *ApJ*, 627, 1001
- van Leeuwen, F. 2007, *A&A*, 474, 653
- Wahhaj, Z., Koerner, D. W., Ressler, M. E., Werner, M. W., Backman, D. E., & Sargent, A. I. 2003, *ApJ*, 584, L27
- Wahhaj, Z., Liu, M. C., Biller, B. A., Clarke, F., Nielsen, E. L., Close, L. M., Hayward, T. L., Mamajek, E. E., Cushing, M., Dupuy, T., Tecza, M., Thatte, N., Chun, M., Ftaclas, C., Hartung, M., Reid, I. N., Shkolnik, E. L., Alencar, S. H. P., Artymowicz, P., Boss, A., de Gouveia Dal Pino, E., Gregorio-Hetem, J., Ida, S., Kuchner, M., Lin, D. N. C., & Toomey, D. W. 2011, *ApJ*, 729, 139
- Wahhaj, Z., Liu, M. C., Biller, B. A., Nielsen, E. L., Close, L. M., Hayward, T. L., Hartung, M., Chun, M., Ftaclas, C., & Toomey, D. W. 2013a, *ApJ*, 779, 80
- Wahhaj, Z., Liu, M. C., Nielsen, E. L., Biller, B. A., Hayward, T. L., Close, L. M., Males, J. R., Skemer, A., Ftaclas, C., Chun, M., Thatte, N., Tecza, M., Shkolnik, E. L., Kuchner, M., Reid, I. N., de Gouveia Dal Pino, E. M., Alencar, S. H. P., Gregorio-Hetem, J., Boss, A., Lin, D. N. C., & Toomey, D. W. 2013b, *ApJ*, 773, 179
- Wang, J. & Ford, E. B. 2011, *MNRAS*, 418, 1822
- Weinberger, A. J., Becklin, E. E., & Zuckerman, B. 2003, *ApJ*, 584, L33
- Zuckerman, B., Song, I., Bessell, M. S., & Webb, R. A. 2001, *ApJ*, 562, L87

Table 1. New Astrometry for β Pic b

Instrument	Filter	Sep. (")	PA ($^{\circ}$)	Epoch (UT)
Gemini/NICI	CH_4S (4%)	0.323 \pm 0.010	209.3 \pm 1.8	2009 Dec 03
Gemini/NICI	CH_4L (4%)	0.339 \pm 0.010	209.2 \pm 1.7	2009 Dec 03
Gemini/NICI	K_S	0.407 \pm 0.005	212.9 \pm 1.4	2010 Dec 25
Gemini/NICI	CH_4S (1%)	0.455 \pm 0.003	211.9 \pm 0.4	2011 Oct 20
Gemini/NICI	K_{cont}	0.452 \pm 0.005	211.6 \pm 0.6	2011 Oct 20
Gemini/NICI	CH_4S (1%)	0.447 \pm 0.003	210.8 \pm 0.4	2012 Mar 29
Gemini/NICI	K_{cont}	0.448 \pm 0.005	211.8 \pm 0.6	2012 Mar 29
Magellan/MagAO+Clio2	3.1 μ m, 3.3 μ m, L' , M'	0.461 \pm 0.014	211.9 \pm 1.2	2012 Dec 02
Magellan/MagAO+VisAO	Y_S	0.470 \pm 0.010	212.0 \pm 1.2	2012 Dec 04

Table 2. Orbital Parameters of β Pic b

Parameter	Lowest χ^2	Median	68% CI	95% CI	GR Stat.
Fixed-Mass					
Semi-major Axis (AU)	9.6	9.1	8.6–14.4	8.2–48.0	1.0827
Eccentricity	0.08	0.08	0.02–0.40	0.00–0.82	1.0580
Inclination Angle ($^{\circ}$)	88.8	88.9	88.2–89.6	87.4–90.4	1.0006
Argument of Periastron ($^{\circ}$)	6.5	-8	-102–85	-167–166	1.0022
Position Angle of Nodes ($^{\circ}$)	211.9	211.8	211.5–212.1	211.2–212.4	1.0011
Epoch of Periastron Passage	2012.88	2012	2009–2019	2006–2023	1.0021
Period (yr)	22.60	21	19–41	18–251	...
Floating-Mass					
Semi-major Axis (AU)	83.6	24.3	9.1–75.2	8.4–96.7	1.2532
Eccentricity	0.90	0.65	0.11–0.89	0.01–0.91	1.2473
Inclination Angle ($^{\circ}$)	89.2	89.0	88.3–89.7	87.6–90.3	1.0047
Argument of Periastron ($^{\circ}$)	347.4	-16	-46–1	-133–116	1.0067
Position Angle of Nodes ($^{\circ}$)	211.6	211.7	211.4–211.9	211.2–212.3	1.0115
Epoch of Periastron Passage	2011.52	2011	2010–2013	2006–2021	1.0012
Period (yr)	581.53	96	22–516	18–758	1.2282
Mass (M_{\odot})	1.73	1.64	1.37–1.95	1.13–2.38	1.0012

Note. — Results from the MCMC fit to the orbit of β Pic b and orbital parameters for the lowest χ^2 within the 68% confidence interval from the chains (Figure 2). The final column gives the Gelman-Rubin statistic for each parameter: values closer to unity indicate a higher degree of convergence.

Table 3. Disk Measurements of β Pic

Disk Component	PA ($^{\circ}$)	Relative Error ($^{\circ}$)	Absolute Error ($^{\circ}$)
NE Outer (60–120 AU)	28.79	0.06	0.3
SW Outer (60–120 AU)	209.21	0.05	0.3
NE Inner (60–90 AU)	32.28	0.07	0.3
SW Inner (60–90 AU)	212.28	0.07	0.3

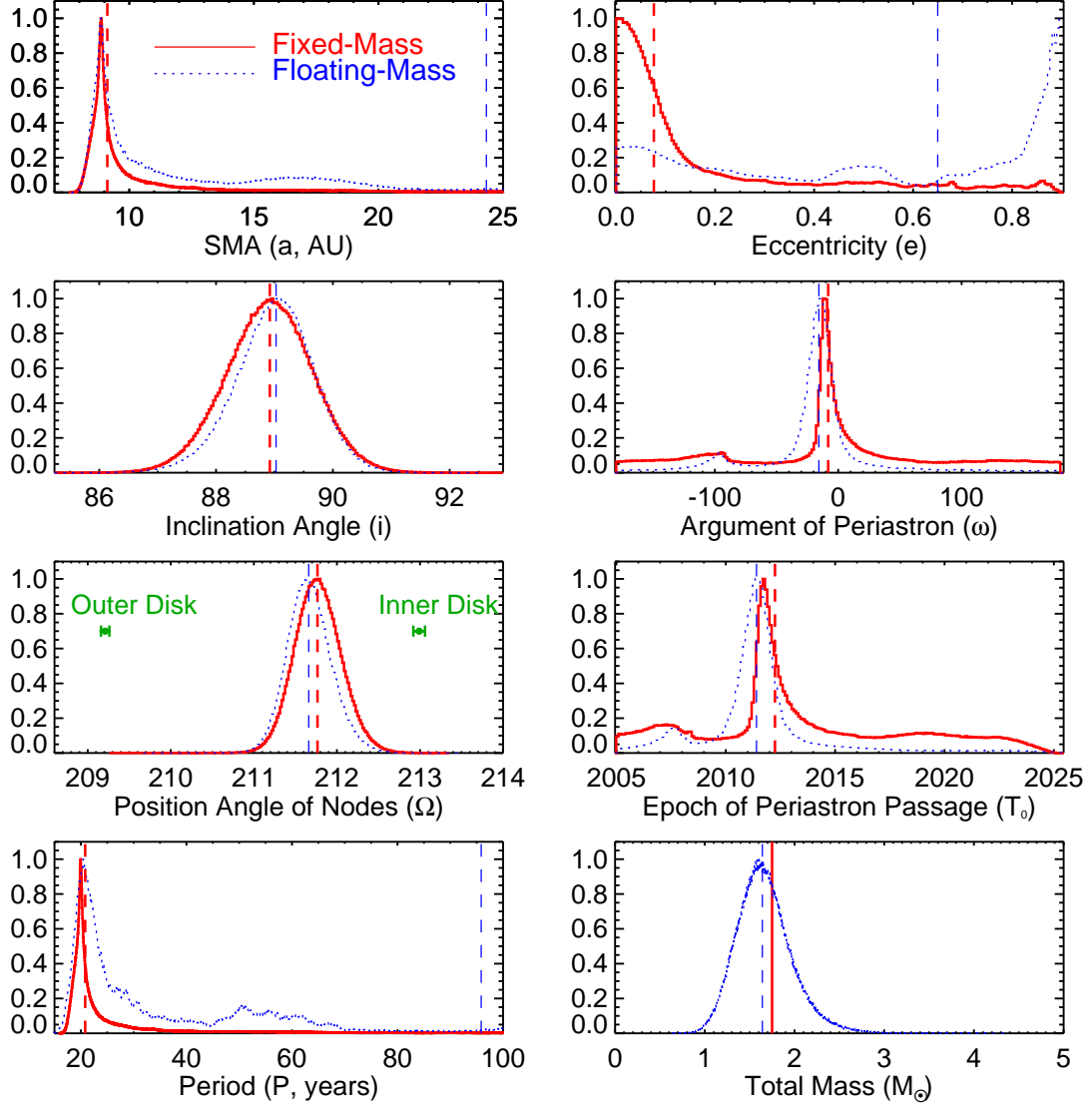


Fig. 1.— Marginalized distributions of orbital parameters from our MCMC fit to the orbit of β Pic b, for the cases where the total mass of the system is fixed at $1.75 M_{\odot}$ (red solid lines) and floating as a free parameter (blue dotted lines). The distributions have been normalized so that their peaks are unity. Dashed lines mark the median of each distribution, and green points and error bars denote the position angle of the outer main disk and inner warped disk, without the overall astrometric calibration error of 0.2° that is common to the measurement of the planet and the two disks. Since the orbital fit draws on data from different instruments, the PDF for position angle of nodes does include the absolute astrometric uncertainties, though (as expected) the uncertainty on the PDF is less than the uncertainty for the PA measurement at any epoch.

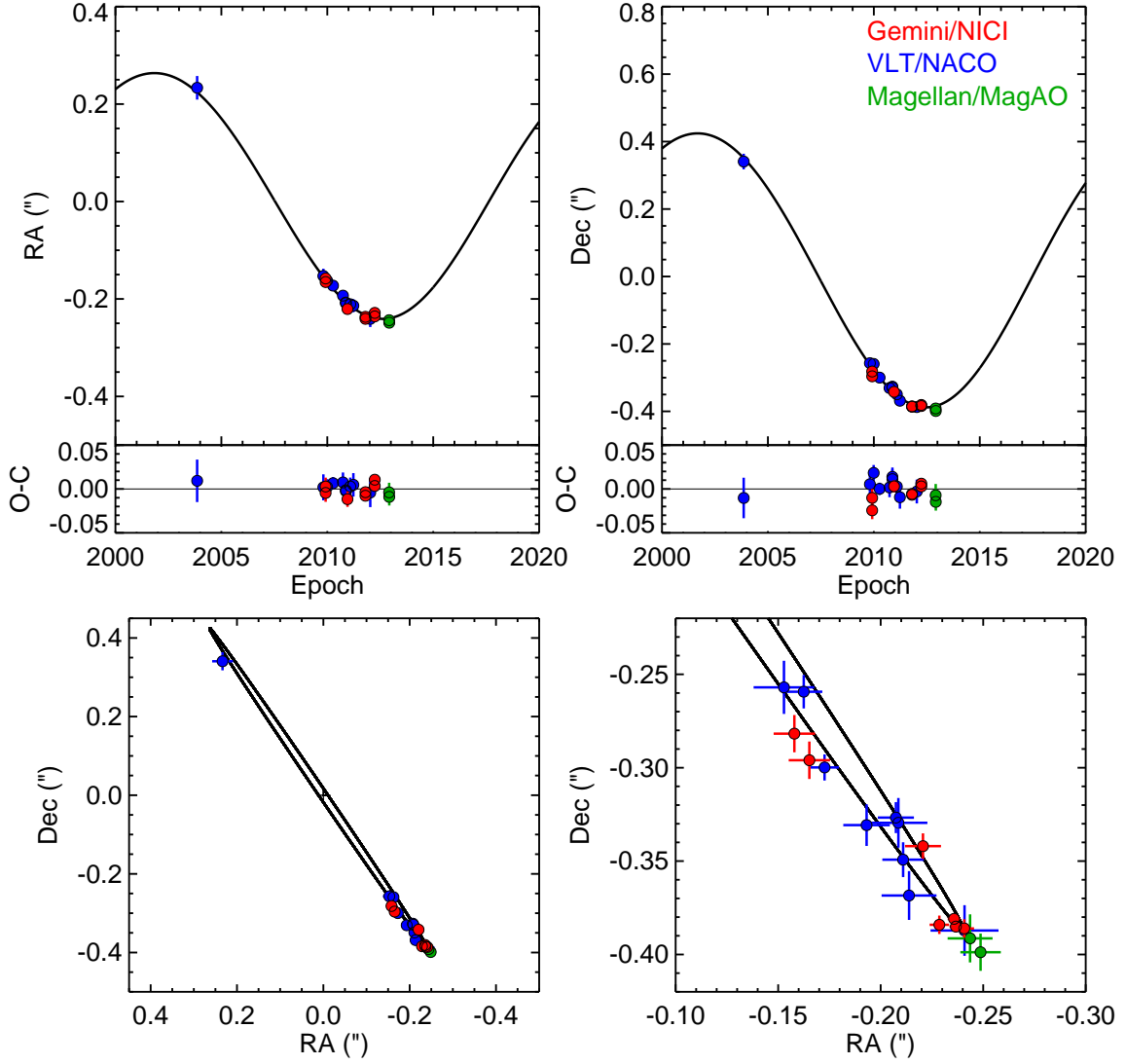


Fig. 2.— The lowest χ^2 orbit within the 68% confidence interval from our fixed-mass MCMC chain, and residuals plotted as Observed - Calculated (O-C), corresponding to a $\chi^2_\nu=1.38$ for 31 degrees of freedom.

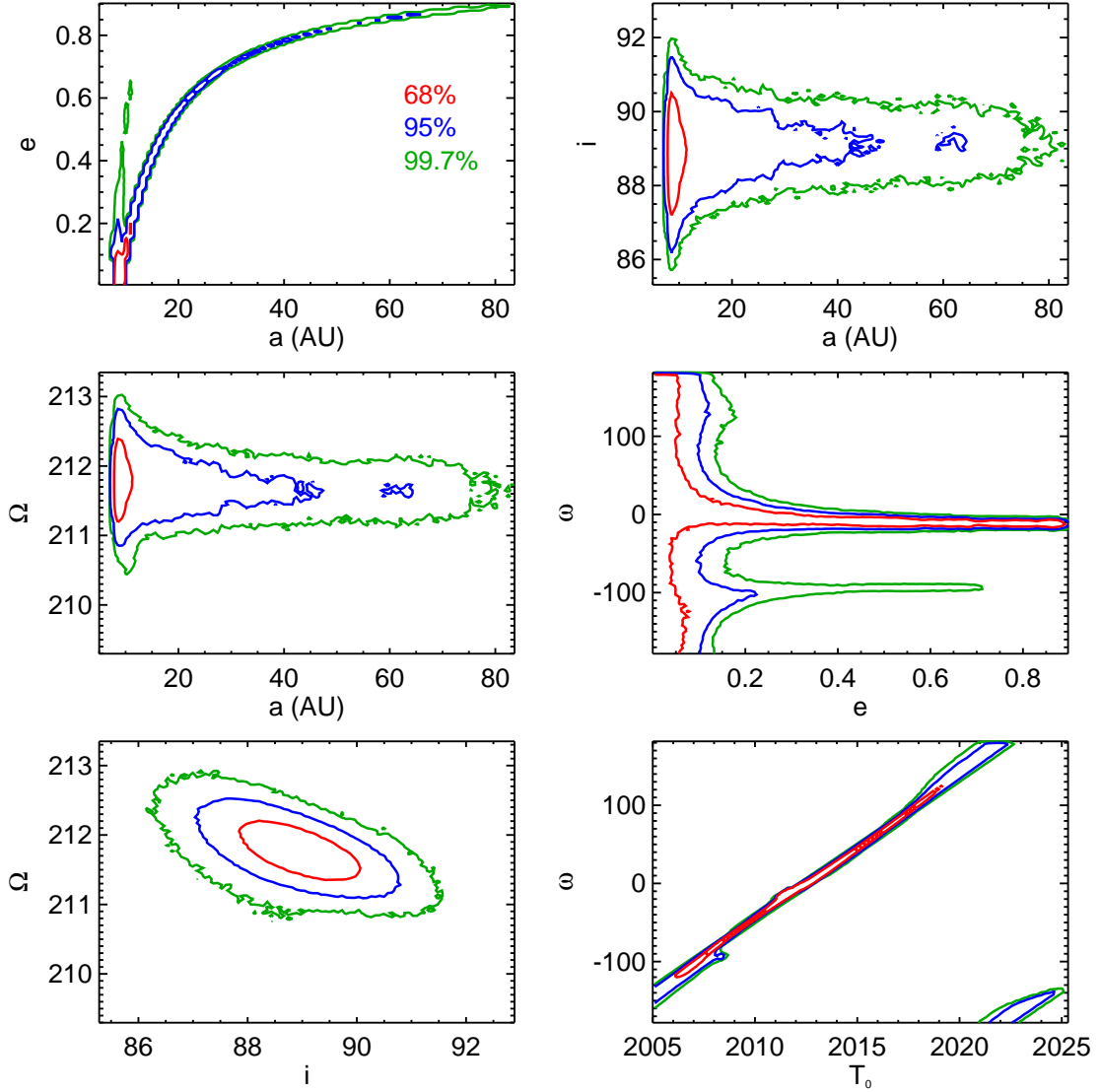


Fig. 3.— Covariances between parameters (semi-major axis a , eccentricity e , inclination angle i , argument of periastron ω , position angle of nodes Ω , and epoch of periastron passage T_0) for the MCMC orbital fit with total mass fixed to $1.75 M_\odot$. Lower semi-major axis corresponds to lower eccentricity, with the most probable orbits close to circular with small semi-major axis. The position angle of nodes and inclination angle are tightly constrained and correlated, with position angle of nodes 3.2σ from the PA inner disk and 7.4σ from the PA of the outer disk.

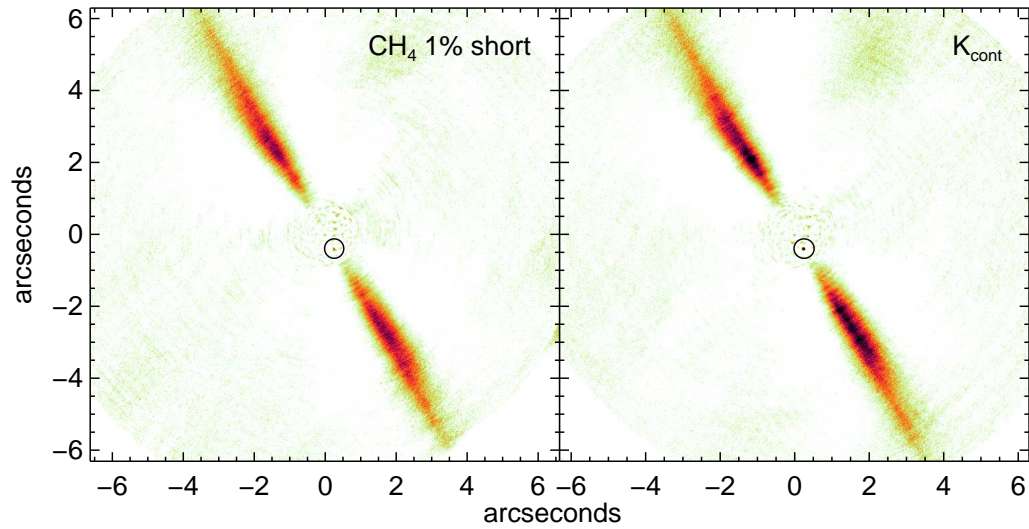


Fig. 4.— Signal-to-noise maps of our Gemini NICI observations of β Pic from 2011 showing both disk and planet in CH_4S (left) and K_{cont} (right). The figure is oriented with North up and East to the left. The black circle marks the location of the planet.